Order online now!

www.rockland.com
tech@rockland.com
+1 484.791.3823

Datasheet for 600-401-383S

DYKDDDDK Tag (Anti-FLAG®) Antibody

Overview

Description:	Antibody for the detection of FLAG® conjugated proteins (RABBIT) - 600-401-383S
Item No.:	600-401-383S
Size:	25 µL
Applications:	ELISA, WB, IF, IHC, IP, Multiplex
Reactivity:	FLAG-Tag
Host Species:	Rabbit

Product Details

Background:	Epitope tags are short peptide sequences that are easily recognized by tag-specific antibodies. Due to their small size, epitope tags do not affect the biochemical properties of the tagged protein. Most often, sequences encoding the epitope tag are included with the target DNA at the time of cloning to produce fusion proteins containing the epitope tag sequence. This allows Anti epitope tag antibodies to serve as universal detection reagents for any tag-containing protein produced by recombinant means. This means that anti-epitope tag antibodies are a useful alternative to generating specific antibodies to identify, immunoprecipitate or immunoaffinity purify a recombinant protein. The anti-epitope tag antibody is usually functional in a variety of antibody-dependent experimental procedures.
Synonyms:	rabbit antibody for the detection of FLAG™ conjugated proteins, rabbit anti DYKDDDDK
Host Species:	Rabbit
Clonality:	Polyclonal
Format:	IgG

Target Details

Reactivity:	FLAG-Tag
Immunogen Type:	Conjugated Peptide
Immunogen:	This antibody was purified from whole rabbit serum prepared by repeated immunizations with the Enterokinase Cleavage Site (ECS) peptide DYKDDDDK (Asp-Tyr-Lys-Asp-Asp-Asp-Asp-Lys) conjugated to KLH using maleimide. This antibody reacts with FLAG™ conjugated proteins.

Purity/Specificity:	This affinity purified antibody is directed against the FLAG™ motif and is useful in determining its presence in various assays. This polyclonal anti-FLAG™ tag antibody detects over-expressed proteins containing the FLAG™ epitope tag. In western blotting of bacterial extracts, the antibody does not cross-react with endogenous proteins.

Application Details

Tested Applications:	ELISA, WB
Suggested Applications:	IF, IHC, IP, Multiplex (Based on references)
Application Note:	This antibody is optimally suited for monitoring the expression of FLAG™ tagged fusion proteins. As such, this antibody can be used to identify fusion proteins containing the FLAG™ epitope. The antibody recognizes the epitope tag fused to either the amino- or carboxy- termini of targeted proteins. This antibody has been tested by ELISA and western blotting against both the immunizing peptide and FLAGä containing recombinant proteins. Although not tested, this antibody is likely functional for immunoprecipitation, immunocytochemistry, and other immunodetection techniques. The epitope tag peptide sequence was first derived from the 11-amino-acid leader peptide of the gene-10 product from bacteriophage T7. Now the most commonly used hydrophilic octapeptide is DYKDDDDK. Rockland Immunochemical's polyclonal antibody to detect FLAG™ conjugated proteins binds FLAG™ containing fusion proteins with greater affinity than the widely used monoclonal M1, M2 and M5 clones, and shows greater sensitivity in most assays. Affinity purification of the polyclonal antibody results in very low background levels in assays and low cross-reactivity with other cellular proteins.
Assay Dilutions:	All assays should be optimized by the user. Recommended dilutions (if any) may be listed below.
ELISA:	1:90,000 - 1:250,000
IHC:	User Optimized
WB:	1:2,000 - 1:10,000

Formulation

Physical State:	Liquid (sterile filtered)
Concentration:	1.09 by UV absorbance at 280 nm
Buffer:	0.02 M Potassium Phosphate, 0.15 M Sodium Chloride, pH 7.2
Preservative:	0.01% (w/v) Sodium Azide
Stabilizer:	None

Shipping & Handling

Shipping Condition:	Dry Ice
Storage Condition:	Store vial at -20° C or below prior to opening. This vial contains a relatively low volume of reagent (25 µL). To minimize loss of volume dilute 1:10 by adding 225 µL of the buffer stated above directly to the vial. Recap, mix thoroughly and briefly centrifuge to collect the volume at the bottom of the vial. Use this intermediate dilution when calculating final dilutions as recommended below. Store the vial at -20°C or below after dilution. Avoid cycles of freezing and thawing.
Expiration:	Expiration date is one (1) year from date of receipt.

Images

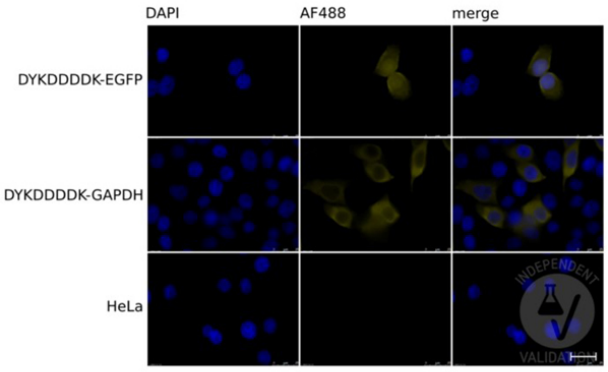

Immunofluorescence Microscopy
Immunofluorescence of the antibody for the detection of FLAG® conjugated proteins.
Cells: HeLa cells transiently expressing DYKDDDDK-tagged EGFP (top row), or GAPDH (middle row), or mock-transfected HeLa cells (bottom row).
Fixation: 4% PFA for 20-30 min at RT.
Primary Antibody: DYKDDDDK Tag antibody diluted 1:200 overnight at 4°C.
Secondary Antibody: chicken anti-rabbit AF488 antibody.
Counterstain: DAPI for 10min at RT.
Staining: DAPI (left column), DYKDDDDK Tag/AF488 (middle column), Merged DAPI and tag staining (right column).
Independently Validated by antibodies-online GmbH (p/n ABIN1043869/ ABIN99294) courtesy of University of Bern.

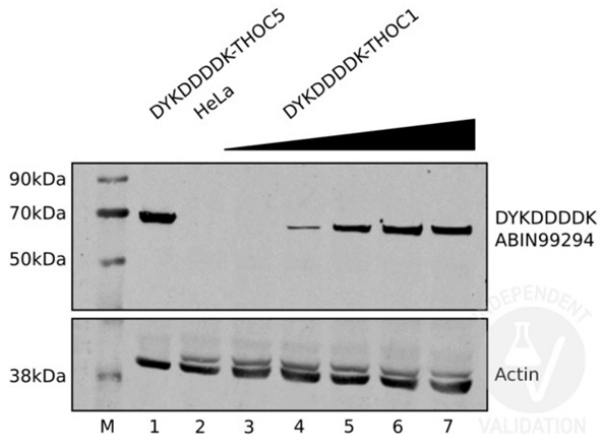

Western Blot
Western Blot of the antibody for the detection of FLAG® conjugated proteins.
Negative Control: (Lane 2) Untransfected HeLa cell extracts.
Positive Control: Transiently expressed DYKDDDDK-tagged THOC5 (lane 1).
Positive Control: Increasing amounts of lysates from HeLa cells transiently expressing DYKDDDDK-tagged THOC1 (lanes 3 to 7).
Primary Antibody: rabbit anti-DYKDDDDK Tag antibody or rabbit anti-actin antibody at 1:2000 for 1h at RT.
Secondary Antibody: IRDye 800CW Goat anti-Rabbit at 1:10000 for 1h at RT.
Independently Validated by antibodies-online GmbH (p/n ABIN1043869/ ABIN99294) courtesy of University of Bern.

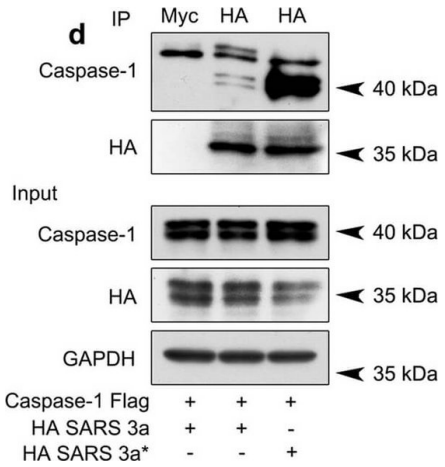

Western Blot

SARS 3a induces NLRP3 inflammasome activation by multiple mechanisms. A) Immunoblot analysis of the pro- and cleaved forms of caspase-1 and IL-1β after reconstitution of inflammasome in HEK 293T cells transfected with SARS 3a with or without NEK7 shRNA. B) Immunoblot analysis of the pro- and cleaved forms of caspase-1 and IL-1β after reconstitution of inflammasome and transfection with SARS 3a or SARS 3a C133A. C) Immunoblot analysis of the pro- and cleaved forms of caspase-1 and IL-1β after co-transfection with caspase-1, IL-1β, and SARS 3a or SARS 3a C133A. D) Immunoprecipitation analysis of interaction between SARS 3a or SARS 3a C133A and caspase-1. All western blot data are representative of two or three independent experiments Figure provided by CiteAb. Source: Cell Death Dis, PMID: 30185776.

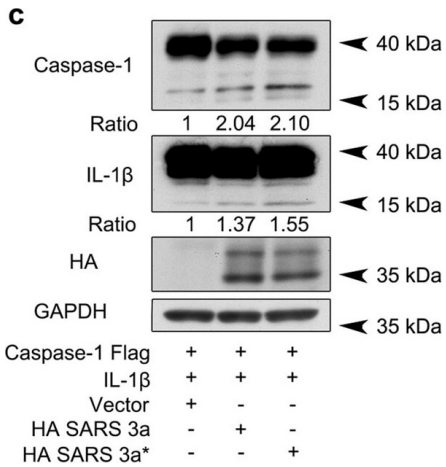

Western Blot

SARS 3a induces NLRP3 inflammasome activation by multiple mechanisms. A) Immunoblot analysis of the pro- and cleaved forms of caspase-1 and IL-1β after reconstitution of inflammasome in HEK 293T cells transfected with SARS 3a with or without NEK7 shRNA. B) Immunoblot analysis of the pro- and cleaved forms of caspase-1 and IL-1β after reconstitution of inflammasome and transfection with SARS 3a or SARS 3a C133A. C) Immunoblot analysis of the pro- and cleaved forms of caspase-1 and IL-1β after co-transfection with caspase-1, IL-1β, and SARS 3a or SARS 3a C133A. D) Immunoprecipitation analysis of interaction between SARS 3a or SARS 3a C133A and caspase-1. All western blot data are representative of two or three independent experiments Figure provided by CiteAb. Source: Cell Death Dis, PMID: 30185776.

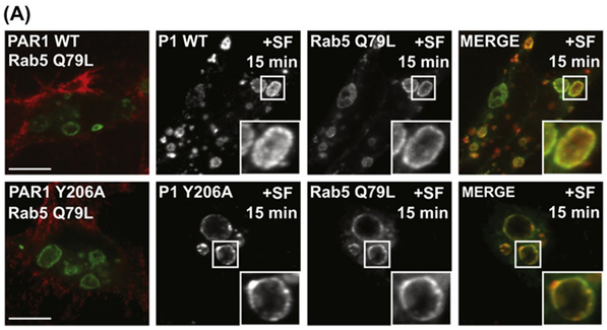

Immunofluorescence Microscopy
Visualization and quantification of GPCR sorting into expanded endosomes. (A) Agonist-stimulated PAR1 sorting into the lumen of expanded endosomes is mediated by the YPXnL motif. HeLa cells expressing FLAG-PAR1 WT or FLAG-PAR1 Y206A were transfected with Rab5-Q79L-GFP, then surface-labeled with anti-FLAG antibody. Cells were stimulated for 15 min with 100 µM SFLLRN, then fixed and analyzed by confocal microscopy. Fig 2. PMID: 26360043

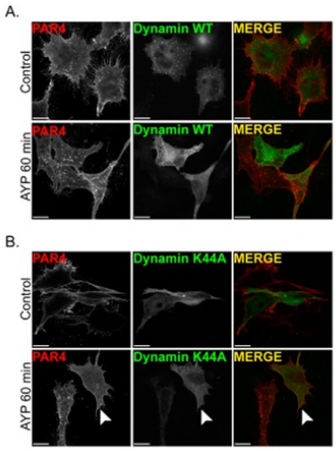

Immunofluorescence Microscopy
Internalization of activated PAR4 occurs through a dynamin- and clathrin-dependent pathway. A and B, HeLa cells transiently transfected with FLAG-PAR4 and either dynamin WT fused to GFP (A) or the dynamin dominant-negative K44A mutant fused to GFP (B) were pre-labeled with anti-FLAG antibody and stimulated with 500 µm AYPGKF for 60 min at 37 °C. Cells were fixed, permeabilized, immunostained, and imaged by confocal microscopy. Arrowheads, dynamin-GFP K44A mutant expressing cells. The images are representative of three independent experiments (scale bar, 10 µm). Fig 1. PMID: 27402844

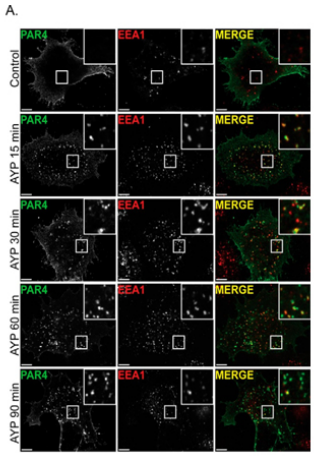

Immunofluorescence Microscopy
Activated PAR4 is internalized and sorted to early endosomes. A, HeLa cells were transfected with FLAG-PAR4, prelabeled with anti-FLAG antibody, stimulated with 500 µm AYPGKF for various times at 37 °C, processed, co-stained with anti-EEA1 antibody, and imaged by confocal microscopy. The images are representative of three independent experiments (scale bar, 10 µm). Insets, magnifications of boxed areas. Fig 2. PMID: 27402844

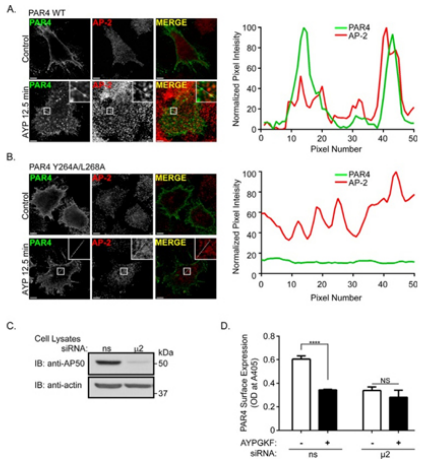

Immunofluorescence Microscopy
AP-2 mediates internalization of activated PAR4. A and B, HeLa cells transfected with FLAG-PAR4 WT (A) or the Y264A/L268A mutant (B) were prelabeled with anti-FLAG antibody, stimulated with 500 µm AYPGKF for 12.5 min at 37 °C, processed, co-stained with anti-AP-2 antibody, and imaged by confocal microscopy. The images are representative of three independent experiments (scale bar, 10 µm). Insets, magnifications of boxed areas. The fluorescence intensity line scans were generated from the regions denoted by the white dashed line in the agonist-stimulated images (A and B, lower panels). C, HeLa cells expressing FLAG-PAR4 were transfected with nonspecific (ns) siRNA or siRNA specific for the µ2 adaptin subunit of AP-2 and immunoblotted (IB) as indicated. D, HeLa cells transfected as described above in C were prelabeled with anti-FLAG antibody and stimulated with 500 µm AYPGKF for 60 min at 37 °C. ELISA was then used to quantify the amount of receptor at the cell surface. Data shown (mean ± S.E.) are representative of three independent experiments, and statistical significance was calculated by two-way ANOVA (****, $p < 0.0001$; ns, not significant). Fig 7. PMID: 27402844

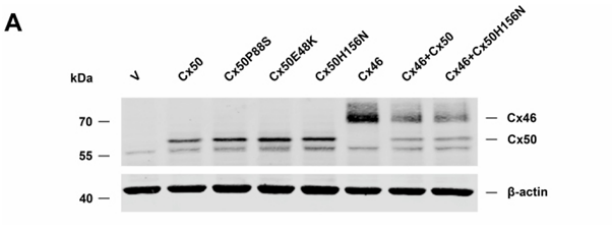

Western Blot
Homomeric and heteromeric HCs formed by Cx50 and Cx46 are induced open by FFSS and inhibited by Cx50 dominant-negative mutants. CEF cells were infected with high-titer RCAS(A) vehicle (V) or recombinant RCAS(A) containing Cx50, Cx50P88S, Cx50E48K, Cx50H156N, Cx46 or co-infected with RCAS(A) containing Cx46 and Cx50 or Cx50H156N. (A) Membrane extracts were immunoblotted with anti-Flag for detecting exogenous Cxs or β-actin as a loading control. Fig 1. PMID: 38820983

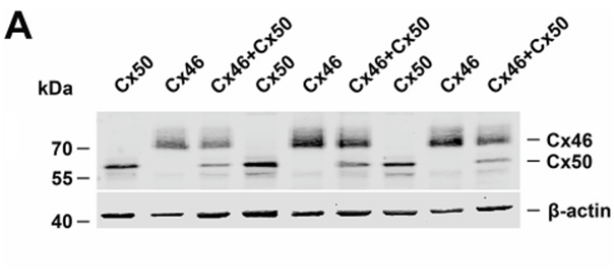

Immunofluorescence Microscopy
Cx50 HCs activated by FFSS have a higher capacity for transporting GSH. (A) CEF cells were infected with high-titer recombinant RCAS(A) retrovirus containing Cx50, Cx46 or co-infected with RCAS(A) containing Cx46 and Cx50. Membrane extracts were immunoblotted with anti-Flag or β-actin antibody. Fig 2. PMID: 38820983

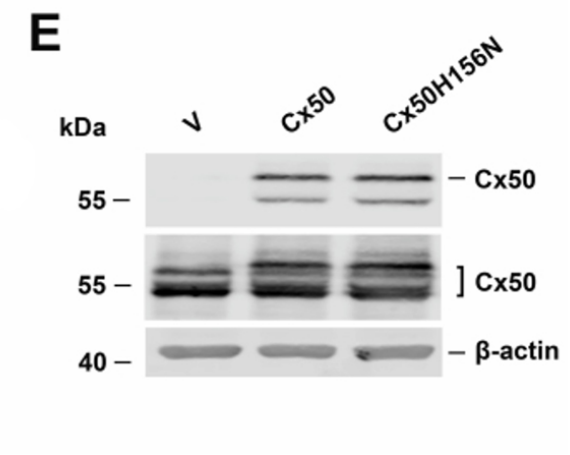

Western Blot
(E) Differentiated lens primary cells were infected with RCAS (A) (V) or recombinant RCAS(A) containing Cx50 or Cx50H156N. Membrane extracts were immunoblotted with anti-Flag, anti-Cx50, or β-actin antibodies. Expression of total (anti-Cx50) and exogenous (anti-Flag) Cx50 was detected. Fig 2. PMID: 38820983

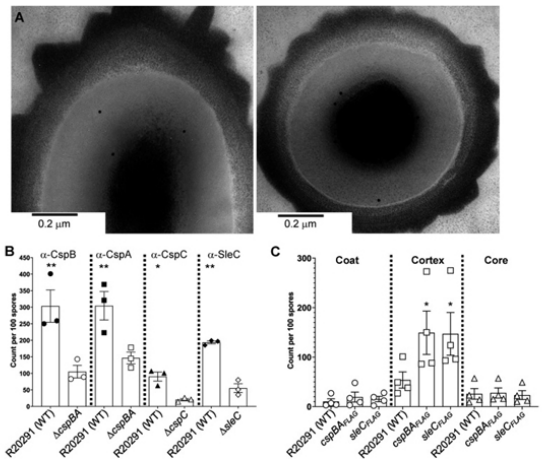

Immunofluorescence Microscopy
CspB, CspA, CspC, and SleC are located within the spore cortex. Spores derived from C. difficile R20291, C. difficile ΔcspBAC, C. difficile ΔsleC, C. difficile ΔcspBAC pcspBAFLAG, and C. difficile ΔsleC psleCFLAG were fixed; embedded in acrylic resins; sectioned; immunolabeled with antibodies specific for the CspB, CspA, CspC, and SleC proteins or the FLAG epitope; and then imaged by TEM. (A) Representative images of anti-FLAG immunolabeled spores derived from the CspBAFLAG (left)- and SleCFLAG (right)-expressing strains. (B) Spores derived from the above-mentioned strains were imaged, and gold particles were counted. For each sample immunolabeled in this way, we imaged 100 random spores on the grid and counted the gold labels present. Counts for the spores derived from the C. difficile R20291, C. difficile ΔcspBAC, and C. difficile ΔsleC strains labeled with anti-CspB, anti-CspA, anti-CspC, and anti-SleC primary and gold-conjugated secondary antibodies. For clarity, only the counts for the gold particles located in the cortex are shown since the counts for the coat layer and the core do not reach statistical significance. Counts were compared to the counts observed in the deletion mutant. (C) Counts for the spores derived from the C. difficile R20291, C. difficile ΔcspBAC pcspBAFLAG, and C. difficile ΔsleC psleCFLAG strains, labeled with anti-FLAG primary and gold-conjugated secondary antibodies, and in various spore regions. The data represent the average from 3 or 4 biological replicates, and the error bars represent the standard errors of the means. **, $P < 0.0001$, and *, $P < 0.05$, as determined by one-way ANOVA using Šidák's multiple-comparison test. An additional, representative, image for each strain can be found in Fig. S1 in the supplemental material. WT, wild type. Fig 6.
PMID: 35762766

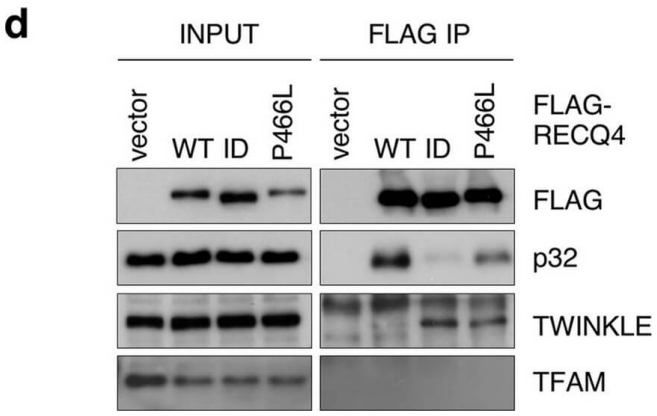

Western Blot

The P466L clinical mutation leads to RECQ4 mitochondrial accumulation. (a) Schematic of human RECQ4 WT, ID and P466L mutant proteins, including the SLD2 (green) and conserved SF2 helicase domains (yellow). (b) Western blot analysis of RECQ4 in WCEs and chromatin-bound (CB) fractions prepared from HEK293 WT or RECQ4 knockdown (KD) HEK293 cells generated by CRISPR technology. Tubulin is used as a loading control. (c) The effects of stable RECQ4 KD shown in (b) and complementation using FLAG-RECQ4 on cell growth as measured by crystal violet cell proliferation assays. Each value represents mean ± standard deviation of 3 independent biological experiments, each with 3 triplicate reactions. (d) Western blot analysis for the presence of WT and mutant FLAG-RECQ4, p32, TWINKLE and TFAM in WCE (left) and immunoprecipitated (IP) with FLAG-RECQ4 complexes (right) in WCEs prepared from stable RECQ4 KD HEK293 cells expressing FLAG-RECQ4 WT, ID or P466L mutant. (e) gDNA levels relative to mtDNA in WCE (left) and MT (right) prepared from stable RECQ4 KD HEK293 cells expressing FLAG-RECQ4 WT, ID or P466L mutant. (f) Western blot analysis of stable RECQ4 KD HEK293 cells expressing FLAG-RECQ4 WT or ID mutant in WCEs and Cyt, MT, and fractions. Tubulin, VDAC1, and lamin A/C are loading and fractionation controls for Cyt, MT, and Nuc fractions, respectively. (g) Western blot analysis of RECQ4 in WCEs and Cyt, MT, and Nuc fractions prepared from stable RECQ4 KD HEK293 cells expressing FLAG-RECQ4 WT or P466L mutant. (h) Representative images showing immunofluorescent staining of FLAG-RECQ4 (green) in stable RECQ4 KD HEK293 cells expressing indicated WT and mutant FLAG-RECQ4 proteins. Mitotracker (red) was used to detect mitochondria, and DAPI (blue) was used to detect nuclei. Figure provided by CiteAb. Source: Sci Rep, PMID: 33046774.

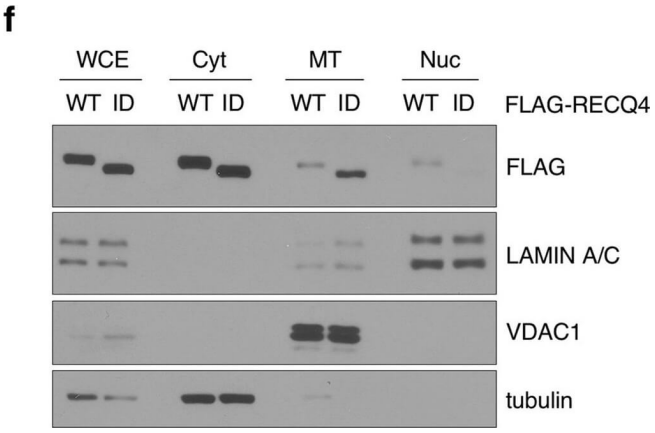

Western Blot

The P466L clinical mutation leads to RECQ4 mitochondrial accumulation. (a) Schematic of human RECQ4 WT, ID and P466L mutant proteins, including the SLD2 (green) and conserved SF2 helicase domains (yellow). (b) Western blot analysis of RECQ4 in WCEs and chromatin-bound (CB) fractions prepared from HEK293 WT or RECQ4 knockdown (KD) HEK293 cells generated by CRISPR technology. Tubulin is used as a loading control. (c) The effects of stable RECQ4 KD shown in (b) and complementation using FLAG-RECQ4 on cell growth as measured by crystal violet cell proliferation assays. Each value represents mean ± standard deviation of 3 independent biological experiments, each with 3 triplicate reactions. (d) Western blot analysis for the presence of WT and mutant FLAG-RECQ4, p32, TWINKLE and TFAM in WCE (left) and immunoprecipitated (IP) with FLAG-RECQ4 complexes (right) in WCEs prepared from stable RECQ4 KD HEK293 cells expressing FLAG-RECQ4 WT, ID or P466L mutant. (e) gDNA levels relative to mtDNA in WCE (left) and MT (right) prepared from stable RECQ4 KD HEK293 cells expressing FLAG-RECQ4 WT, ID or P466L mutant. (f) Western blot analysis of stable RECQ4 KD HEK293 cells expressing FLAG-RECQ4 WT or ID mutant in WCEs and Cyt, MT, and fractions. Tubulin, VDAC1, and lamin A/C are loading and fractionation controls for Cyt, MT, and Nuc fractions, respectively. (g) Western blot analysis of RECQ4 in WCEs and Cyt, MT, and Nuc fractions prepared from stable RECQ4 KD HEK293 cells expressing FLAG-RECQ4 WT or P466L mutant. (h) Representative images showing immunofluorescent staining of FLAG-RECQ4 (green) in stable RECQ4 KD HEK293 cells expressing indicated WT and mutant FLAG-RECQ4 proteins. Mitotracker (red) was used to detect mitochondria, and DAPI (blue) was used to detect nuclei. Figure provided by CiteAb. Source: Sci Rep, PMID: 33046774.

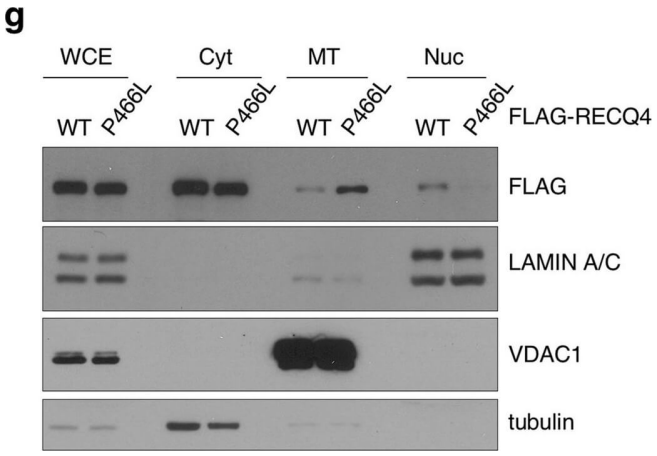

Western Blot

The P466L clinical mutation leads to RECQ4 mitochondrial accumulation. (a) Schematic of human RECQ4 WT, ID and P466L mutant proteins, including the SLD2 (green) and conserved SF2 helicase domains (yellow). (b) Western blot analysis of RECQ4 in WCEs and chromatin-bound (CB) fractions prepared from HEK293 WT or RECQ4 knockdown (KD) HEK293 cells generated by CRISPR technology. Tubulin is used as a loading control. (c) The effects of stable RECQ4 KD shown in (b) and complementation using FLAG-RECQ4 on cell growth as measured by crystal violet cell proliferation assays. Each value represents mean ± standard deviation of 3 independent biological experiments, each with 3 triplicate reactions. (d) Western blot analysis for the presence of WT and mutant FLAG-RECQ4, p32, TWINKLE and TFAM in WCE (left) and immunoprecipitated (IP) with FLAG-RECQ4 complexes (right) in WCEs prepared from stable RECQ4 KD HEK293 cells expressing FLAG-RECQ4 WT, ID or P466L mutant. (e) gDNA levels relative to mtDNA in WCE (left) and MT (right) prepared from stable RECQ4 KD HEK293 cells expressing FLAG-RECQ4 WT, ID or P466L mutant. (f) Western blot analysis of stable RECQ4 KD HEK293 cells expressing FLAG-RECQ4 WT or ID mutant in WCEs and Cyt, MT, and fractions. Tubulin, VDAC1, and lamin A/C are loading and fractionation controls for Cyt, MT, and Nuc fractions, respectively. (g) Western blot analysis of RECQ4 in WCEs and Cyt, MT, and Nuc fractions prepared from stable RECQ4 KD HEK293 cells expressing FLAG-RECQ4 WT or P466L mutant. (h) Representative images showing immunofluorescent staining of FLAG-RECQ4 (green) in stable RECQ4 KD HEK293 cells expressing indicated WT and mutant FLAG-RECQ4 proteins. Mitotracker (red) was used to detect mitochondria, and DAPI (blue) was used to detect nuclei. Figure provided by CiteAb. Source: Sci Rep, PMID: 33046774.

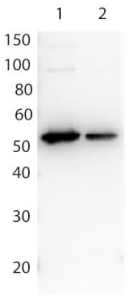

Western Blot
Affinity Purified Antibody to detect FLAG conjugated proteins detects both C terminal linked and N terminal linked FLAG tagged recombinant proteins by western blot. This antibody was used at a dilution of 1:1,000 to detect 0.1 µg of recombinant protein containing either the FLAG epitope tag linked at the carboxy (C), Lane 2, or the amino (N), Lane 1, terminus of the recombinant protein. A 4-20% gradient gel was used to resolve the protein by SDS-PAGE. The protein was transferred to nitrocellulose using standard methods. After blocking, the membrane was probed with the primary antibody overnight at 4°C followed by washes and reaction with a 1:40,000 dilution of HRP conjugated Gt-a-Rabbit IgG (H&L) MX10 (code 611-103-122) for 30 min at room temperature. Bio-Rad's VersaDoc® 4000 MP Imaging System was used to process the image. Other detection systems will yield similar results

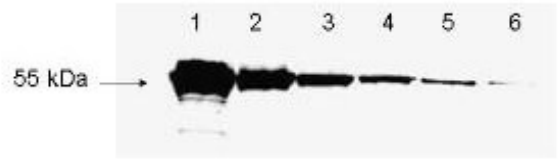

Western Blot
Rockland's antibody to detect FLAG™ conjugated proteins is shown to detect as little as 3 ng of amino-terminal FLAG™ tagged recombinant protein by western blot. This antibody was used at a 1:1,000 dilution to detect 3-fold serial dilutions of amino-terminal FLAG™-Bacterial Alkaline Phosphatase (BAP) fusion protein (Sigma P-7582) starting at 1.0 µg of protein as shown in lanes 1-6 respectively. A 4-20% gradient gel was used to separate the protein by SDS-PAGE. The protein was transferred to nitrocellulose using standard methods. After blocking, the membrane was probed with the primary antibody for 1 h at room temperature followed by washes and reaction with a 1:10,000 dilution of IRDye® 800 conjugated Gt-a-Rabbit IgG (H&L) (code 611-132-122) for 30 min at room temperature. LICOR's Odyssey® Infrared Imaging System was used to scan and process the image. Other detection systems will yield similar results

Western Blot
Western Blot of Rabbit anti-FLAG antibody. Marker: Opal Pre-stained ladder (p/n MB-210-0500). Lane 1: HEK293 lysate (p/n W09-000-365). Lane 2: HeLa Lysate (p/n W09-000-364). Lane 3: CHO/K1 Lysate (p/n W07-000-357). Lane 4: MDA-MB-231 (p/n W09-001-GK6). Lane 5: A431 Lysate (p/n W09-000-361). Lane 6: Jurkat Lysate (p/n W09-001-370). Lane 7: NIH/3T3 Lysate (p/n W10-000-358). Lane 8: E-coli HCP Control (p/n 000-001-J08). Lane 9: FLAG Positive Control Lysate (p/n W00-001-383). Lane 10: Red Fluorescent Protein (p/n 000-001-379). Lane 11: Green Fluorescent Protein (p/n 000-001-215). Lane 12: Glutathione-S-Transferase Protein. Lane 13: Maltose Binding Protein (p/n 000-001-385). Load: 10 µg of lysate or 50ng of purified protein per lane. Primary antibody: FLAG antibody at 1ug/mL overnight at 4C. Secondary antibody: Peroxidase rabbit secondary antibody (p/n 611-103-122) at 1:30,000 for 60 min at RT. Blocking Buffer: 1% Casein-TTBS for 30 min at RT. Predicted/Observed size: 55 kDa for FLAG.

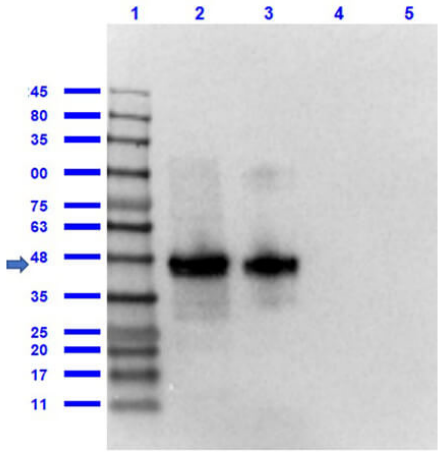

Western Blot
Western Blot of Rabbit anti-FLAG antibody. Lane 1: Opal Prestained Molecular Weight Marker (p/n MB-210-0500). Lane 2: FLAG Positive Control Lysate (p/n W00-E01-383) (10µg) [+]. Lane 3: 12 Epitope GST Tagged Lysate (p/n MB-302-0100) (10µg) [+]. Lane 4: rGST protein (p/n 000-001-200) (0.1µg) [-]. Lane 5: MBP protein (p/n 000-001-385) (0.1µg) [-]. Primary Antibody: Anti-FLAG at 1.0 µg/mL overnight at 2-8°C. Secondary Antibody: Goat Anti-Rabbit IgG Peroxidase (p/n 611-103-122) at 1:70,000 at RT for 30 mins. Block: BlockOut Buffer (p/n MB-073). Predicted MW: ~55kDa. Observed MW: ~48kDa. Exposure: 2 sec.

References

- Pintor K et al. In situ analysis of type III secretion chaperone proteins indicates a cytosolic handover of virulence effectors. *FEMS Microbes.* (2025)
- Lacey TA et al. Kv2/Kv6.4 Heteromeric Potassium Channels Are Expressed in Spinal Motoneurons and Localized at C-Bouton Synapses. *Eur J Neurosci.* (2025)
- Cbrianceau C et al. Continuous exchange of an inner-membrane ring component is required for assembly and function of the type III secretion system. *Nat Commun.* (2025)

- Wen MH et al. Elevated intracellular copper induces CTR1 monomerization and prevents copper uptake. *Nat Commun.* (2025)
- Tong Y et al. Mechano-activated connexin hemichannels and glutathione transport protect lens fiber cells against oxidative insults. *Redox Biol.* (2024)
- Morales AE et al. Wilms' tumor 1 (WT1) antigen is overexpressed in Kaposi Sarcoma and is regulated by KSHV vFLIP. *PLoS Pathog.* (2024)
- Fujii S et al. Redox states in the endoplasmic reticulum directly regulate the activity of calcium channel, inositol 1,4,5-trisphosphate receptors. *Proc Natl Acad Sci U S A.* (2023)
- Herfurth M et al. A miniTurbo-based proximity labeling protocol to identify conditional protein interactomes in vivo in Myxococcus xanthus. *STAR Protoc.* (2023)
- Uegaki K et al. The oxidative folding of nascent polypeptides provides electrons for reductive reactions in the ER. *Cell Rep.* (2023)
- Geng S et al. A conserved RWP-RK transcription factor VSR1 controls gametic differentiation in volvocine algae. *Proc Natl Acad Sci U S A.* (2023)
- Acosta FM et al. Microinjection of Recombinant RCAS(A) Retrovirus into Embryonic Chicken Lens. *J Vis Exp.* (2023)
- Chen H et al. Probing Oxidant Effects on Superoxide Dismutase 1 Oligomeric States in Live Cells Using Single-Molecule Fluorescence Anisotropy. *Chem Biomed Imaging.* (2023)
- Li Z et al. The second extracellular domain of connexin 50 is important for in cell adhesion, lens differentiation, and adhesion molecule expression. *J Biol Chem.* (2023)
- Baloh M et al. Imaging Clostridioides difficile Spore Germination and Germination Proteins. *J Bateriol.* (2022)
- Montes-Bravo N et al. Role of the Spore Coat Proteins CotA and CotB, and the Spore Surface Protein CDIF630_02480, on the Surface Distribution of Exosporium Proteins in Clostridioides difficile 630 Spores. *Microorganisms.* (2022)
- Hayashi T et al. Ubiquitin-dependent rapid degradation conceals a cell-protective function of cytoplasmic SIRT3 against oxidative stress. *J Biochem.* (2022)
- Fusi L et al. Interaction of transcription factor FoxO3 with histone acetyltransferase complex subunit TRRAP Modulates Gene Expression and Apoptosis. *J Biol Chem.* (2022)
- Nabar NR et al. LRRK2 is required for CD38-mediated NAADP-Ca2+ signaling and the downstream activation of TFEB (transcription factor EB) in immune cells. *Autophagy.* (2022)
- Wang Y et al. Molecular mechanism of RIPK1 and caspase-8 in homeostatic type I interferon production and regulation. *Cell Rep.* (2022)
- Häusl, AS et al. Mediobasal hypothalamic FKBP51 acts as a molecular switch linking autophagy to whole-body metabolism. *Science Advances* (2022)
- Carr HS et al. The PDZ domain protein SYNJ2BP regulates GRK-dependent Sst2A phosphorylation and downstream MAPK signaling. *Endocrinology.* (2021)
- Schnitzler L et al. Lensless digital holographic microscopy as an efficient method to monitor enzymatic plastic degradation. *Mar Pollut Bull.* (2021)

- Chang Y et al. Analysis of the TORC1 interactome reveals a spatially distinct function of TORC1 in mRNP complexes. *J Cell Biol.* (2021)
- Haines A et al. Cross Talk between ARF1 and RhoA Coordinates the Formation of Cytoskeletal Scaffolds during Chlamydia Infection. *mBio.* (2021)
- Herrera-Cruz MS et al. Rab32 uses its effector reticulon 3L to trigger autophagic degradation of mitochondria-associated membrane (MAM) proteins. *Biol Direct.* (2021)
- Martinelli S et al. Stress-primed secretory autophagy promotes extracellular BDNF maturation by enhancing MMP9 secretion. *Nat Commun.* (2021)
- Li Z et al. Development of a potent embryonic chick lens model for studying congenital cataracts in vivo. *Commun Biol.* (2021)
- De Giorgi M et al. Targeting the Apoa1 locus for liver-directed gene therapy. *Mol Ther Methods Clin Dev.* (2021)
- Skotnicka, D et al. CdbA is a DNA-binding protein and c-di-GMP receptor important for nucleoid organization and segregation in Myxococcus xanthus. *Nature Communications* (2020)
- Lindner F et al. LITESEC-T3SS-Light-controlled protein delivery into eukaryotic cells with high spatial and temporal resolution. *Nat Commun.* (2020)
- Treuner-Lange A et al. PilY1 and minor pilins form a complex priming the type IVa pilus in Myxococcus xanthus. *Nat Commun.* (2020)
- Chang CW et al. Pathogenic mutations reveal a role of RECQ4 in mitochondrial RNA: DNA hybrid formation and resolution. *Sci Rep.* (2020)
- Liu J et al. Mechanosensitive collaboration between integrins and connexins allows nutrient and antioxidant transport into the lens. *J Cell Biol.* (2020)
- Sadek J, Wuo MG, Rooklin D, et al. Modulation of virus-induced NF-κB signaling by NEMO coiled coil mimics. *Nat Commun.* (2020)
- Duan, G et al. Robust Antibacterial Activity of Tungsten Oxide (WO3-x) Nanodots. *Chemical Research in Toxicology* (2019)
- Terra LF et al. Heat shock protein B1 is a key mediator of prolactin-induced beta-cell cytoprotection against oxidative stress. *Free Radic Biol Med.* (2019)
- Olsen C et al. Regulation of somatostatin receptor 2 trafficking by C-tail motifs and the retromer. *Endocrinology.* (2019)
- Zannas AS et al. Epigenetic derepression of FKBP5 by aging and stress contributes to NF-κB-driven inflammation and cardiovascular risk. *Proc Natl Acad Sci USA* (2019)
- Lucarelli et al. Resolving the Combinatorial Complexity of Smad Protein Complex Formation and Its Link to Gene Expression. *Cell Systems* (2018)
- Geng et al. Evolutionary divergence of the sex-determining gene MID uncoupled from the transition to anisogamy in volvocine algae. *Development* (2018)
- Shimo et al. Construction of a tri-chromatic reporter cell line for the rapid and simple screening of splice-switching oligonucleotides targeting DMD exon 51 using high content screening. *PLOS One* (2018)
- Yue et al. SARS-Coronavirus Open Reading Frame-3a drives multimodal necrotic cell death. *Cell Death & Disease* (2018)

- Smith et al. Protease-activated receptor-4 and P2Y12 Dimerize, Co-Internalize and Activate Akt Signaling via Endosomal Recruitment of β-arrestin. *Journal of Biological Chemistry* (2017)
- Hu et al. Connexin 50 Functions as an Adhesive Molecule and Promotes Lens Cell Differentiation. *Scientific Reports* (2017)
- Sleven H et al. De novo mutations in EBF3 cause a neurodevelopmental syndrome. *Am J Hum Genet.* (2017)
- Grimsey et al. Recycling and Endosomal Sorting of Protease-activated Receptor-1 Is Distinctly Regulated by Rab11A and Rab11B Proteins. *Journal of Biological Chemistry* (2016)
- Wang et al. S6K-STING interaction regulates cytosolic DNA-mediated activation of the transcription factor IRF3. *Nature Immunology* (2016)
- Smith et al. Protease-activated Receptor-4 Signaling and Trafficking Is Regulated by the Clathrin Adaptor Protein Complex-2 Independent of β-Arrestins. *Journal of Biological Chemistry* (2016)
- Gassen NC et al. FKBP51 inhibits GSK3β and augments the effects of distinct psychotropic medications. *Mol Psychiatry.* (2015)
- Dores MR et al. GPCR sorting at multivesicular endosomes. *Methods Cell Biol.* (2015)
- Gassen NC et al. Chaperoning epigenetics: FKBP51 decreases the activity of DNMT1 and mediates epigenetic effects of the antidepressant paroxetine. *Sci Signal.* (2015)
- Ortiz-Sandoval CG. Et al. Interaction with the effector dynamin-related protein 1 (Drp1) is an ancient function of Rab32 subfamily proteins. *Cell Logist.* (2014)
- Sinha S et al. Essential role of the chaperonin CCT in rod outer segment biogenesis. *Invest Opthalmol. Vis Sci.* (2014)
- Liggett J et al. A novel COX-independent mechanism of sulindac sulfide involves cleavage of epithelial cell adhesion molecule protein. *Exp Cell Res.* (2014)
- Dege C et al. Mi-2/NuRD chromatin remodeling complexes regulate B and T-lymphocyte development and function. *Immunol Rev.* (2014)
- Gassen NC et al. Association of FKBP51 with priming of autophagy pathways and mediation of antidepressant treatment response: evidence in cells, mice, and humans. *PLoS Med.* (2014)
- Gao X et al. Splice isoforms of phosducin-like protein control the expression of heterotrimeric G proteins. *J Biol Chem.* (2013)
- Hara H et al. Phosphorylation of the adaptor ASC acts as a molecular switch that controls the formation of speck-like aggregates and inflammasome activity. *Nat Immunol.* (2013)
- Badeaux AI et al. Loss of the methyl lysine effector protein PHF20 impacts the expression of genes regulated by the lysine acetyltransferase MOF. *Biol Chem.* (2012)
- Raghavan B et al. Metal allergens nickel and cobalt facilitate TLR4 homodimerization independently of MD2. *EMBO Rep.* (2012)
- Petersen B et al. Transgenic expression of human heme oxygenase-1 in pigs confers resistance against xenograft rejection during ex vivo perfusion of porcine kidneys. *Xenotransplantation.* (2011)
- Albus CA et al. Y3IP1, a nucleus-encoded thylakoid protein, cooperates with the plastid-encoded Ycf3 protein in photosystem I assembly of tobacco and Arabidopsis. *Plant Cell.* (2010)

www.rockland.com
tech@rockland.com
+1 484.791.3823

Disclaimer

This product is for research use only and is not intended for therapeutic or diagnostic applications. Please contact a technical service representative for more information. All products of animal origin manufactured by Rockland Immunochemicals are derived from starting materials of North American origin. Collection was performed in United States Department of Agriculture (USDA) inspected facilities and all materials have been inspected and certified to be free of disease and suitable for exportation. All properties listed are typical characteristics and are not specifications. All suggestions and data are offered in good faith but without guarantee as conditions and methods of use of our products are beyond our control. All claims must be made within 30 days following the date of delivery. The prospective user must determine the suitability of our materials before adopting them on a commercial scale. Suggested uses of our products are not recommendations to use our products in violation of any patent or as a license under any patent of Rockland Immunochemicals, Inc. If you require a commercial license to use this material and do not have one, then return this material, unopened to: Rockland Inc., P.O. BOX 5199, Limerick, Pennsylvania, USA.